ISSN: 2639-7455

Research Article

Earth & Environmental Science Research & Reviews

Integration of Advection and Mixing Using Fluid Mass-Momentum-Covering Relationships

Zhiren Wang

Institute of Marine and Coastal Sciences, Rutgers, The State University of New Jersey

***Corresponding author**
Zhiren Wang, Institute of Marine and Coastal Sciences, Rutgers, The State University of New Jersey, 71 Dudley Road, New Brunswick, NJ 08901; Email: joewwh77@gmail.com

Submitted: 10 Jan 2019; **Accepted**: 17 Jan 2019; **Published**: 02 Mar 2019

Abstract

Classical discretization of discrete fluids and parameterization of mixing bring modeling uncertainties for momentum-uneven fluids by setting the grid spacing as the distance for fluids to move within one time step, using low resolutions, and introducing dozens of parameters dependent of scales and modeling processes. Low resolutions have linearized, in a rather extent, nonlinear motions and failed to forecast accelerations that can cause climate adjustments, especially during solving tide-associated dynamics. Here, I wrote Newton Law directly for discrete fluids under conservations of momentum and mass using "mass and momentum-covering relationships (MMCR)", and combined advection and mixing terms. Mixing became a higher-order advection terms induced from speed gradients times coefficients that are functions of density, grid spacing, and the gradients of speed, density and momentum. Parameterization can be avoided and no uncertain parameters are involved in modeling. Preliminary modeling experiments showed skill for simulation of sea surface temperatures over tropical oceans where momentum was more uneven than as compared with higher latitudes.

Keyword: mixing, advection, mass and momentum-covering relationships, integration of advection and mixing, climate modeling

Note: This paper is, a fraction of my book titled "Preliminary studies of climate-environment dynamics for our Climate Prediction and Environment" is for contributing to climate-environment studies and prediction [1].

Introduction

Mixing is important for not only circulations but also for tracer and energy transports. A small fraction kinetic energy from circulations can transport huge amount of energy and changes in directions or magnitudes of circulations may cause large weather-climate adjustment [2]. Dozens of experimental parameters have to be adjusted for mixing according to modeling methods and domains. Mixing schemes are scale-dependent, e.g., with M-Y used for small scales and KPP used for large scales [3-6]. As the major mixing component in circulation modeling, vertical mixing process has been explored with numerous mixing schemes but still with a long-standing challenge for accurate parameterization [7-13].

The field theory applied in the classical fluid mechanics describes continuous fluids accurately without mixing terms [14-15]. The mixing terms come up in momentum-uneven or discrete fluids. Discretization uses the mean state within grids to replace the state at one point and equivalently linearize the kinetic equations in some extent, and large-scale numerical models of lower spatial resolutions are inadequate to resolve the internal tides with shorter wavelengths and the sub-grid processes such as eddies for momentum-uneven fluids, as shown in this study. Although momentum-unevenness produces gradients (e.g., accelerations) and may cause adjustment to a climate system, the momentum-unevenness is often smoothed out and treated as "noises" through smoothing and filters that are widely employed in numerical processes during climate modeling [16-18]. Numerical simulation effects are dependent of temporal and spatial resolutions and models lacked skill in simulating and predicting the sea surface temperature (SST) in the tropical Pacific Ocean where the momentum was more uneven, which imply uncertainties in mixing [19].

Uncertainties in mixing may result from multiple approximations (see Section 2 for details). Large domain models objectively need different mixing schemes especially where multiple resolutions are applied. Can uncertainties in mixing be avoided through avoiding parameterizations and integrating mixings and advection? This study integrated mixing and advection using the mass and momentum-covering relationships (MMCR) of fluids through a direct application of momentum law in discrete fluids, generalizing mixings for all scales in multi-resolution modeling (see Section 3 for details), followed with a modeling examination for the preliminary effects using the MMCR (see Section 4 for details).

Methods

Uncertainties in mixing may result from multiple approximations during discretization of momentum equations for fluids. Mathematical misrepresentation and linearization during discretization, insufficient

resolutions of numerical models, and well-posed contradiction for discrete space as well as local parameterizations for subscale behaviors with various closures and other numerical modeling processes such as smoothing and filter may be the typical approximations that cause uncertainties in mixing.

Mathematical misrepresentation and linearization during discretization

Lagrangian and Eulerian forms of kinetic equations can be equivalently transferred in ideal, mathematically continuous space

$$\frac{dV[s(t),t]}{dt} = \frac{\partial V}{\partial t} + \frac{\partial V}{\partial s}\frac{\partial s}{\partial t} = F \quad (1)$$

The general discrete form of the Eulerian kinetic equation should be

$$\frac{\Delta_t V}{\Delta t} + \frac{\Delta_s V}{\Delta s}\frac{\Delta s}{\Delta t} = F \quad (2)$$

Where $\vec{V}$ is speed in $\vec{I}_s$ (unit vector) direction, $\frac{\partial s}{\partial t} \equiv \vec{V} \bullet \vec{I}_s = V$, Δs is the distance for the local fluid to move within [t, $t+\Delta t$], $\Delta_t V$ and $\Delta_s V$ are the increments of V in Δt and Δs , respectively, F is force.

There are two mathematical preconditions for the discretization as shown below

$$\frac{\Delta s}{\Delta t} \equiv V \quad (3)$$

$$\Delta s \equiv \int_t^{t+\Delta t} V\, dt \quad (4)$$

For the nonlinear fluids, however, these two mathematical preconditions were not met because of the follows: First, $\frac{\Delta s}{\Delta t} = \frac{1}{\Delta t}\int_t^{t+\Delta t} V\, dt = V$ condition was not always satisfied unless V is constant within each of the time steps [t, $t+\Delta t$]. Second, Δs is not the distance for the local fluid to move within one time stepΔt, instead it is set as the grid spacing. That using V as constant within each of the time steps or setting Δs as the grid spacing during numerical computation is using the mean state within each of the time steps or grid spacing to replace the real state at one temporal or spatial point, making the model dependent of its temporal and spatial resolution and linearizing the system in some extent if the system is a nonlinear one. The temporal or spatial deformation with large gradients would be missed during the numerical computation and fail accurate prediction for the climate adjustment because large gradients including accelerations cause climate adjustment. At local points, the real gradients can be much stronger than that averaged within entire grids (Fig. 1). Grid spacing is often much larger than the distance the fluid covers within one time step, making the "linearization" unavoidable in large-scale climate model. Meaning, smoothing, and filtering in models enhance the "linearization".

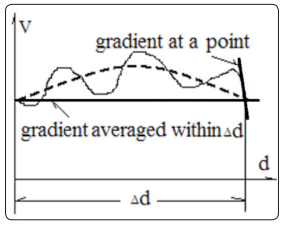

Figure 1: Diagram showing that a gradient at a local point can be much larger than the gradient averaged within a time step (d = t) or grid spacing (d = s).

Insufficient resolutions of numerical models

The two mathematical preconditions require much high resolutions with the Δt and Δs small enough and require small accelerations in order to make the mean within grids approach its real value gradient at local points. However, resolutions of large-scale numerical models were insufficient to have accurate solutions for tide-associated dynamics, which can be demonstrated through two obvious cases in follows:

Case one on the internal tidal-forced waves: Suppose the $\Delta s / \Delta t = V$ is accepted in discretization, the discrete form of Equation 2 can be written as

$$\frac{\Delta_t V}{\Delta t} + \frac{\Delta_s V}{\Delta s}\frac{\Delta s}{\Delta t} \approx \frac{\Delta_t V}{\Delta t} + V\frac{\Delta_s V}{\Delta s} \quad (5)$$

The internal tidal-forced waves in s-direction with wave speed (c) and wavelength (L) can be written as $V = V_o \sin[\frac{2\pi}{L}(s-ct)]$. Applying a Taylor series expansion, the absolute speed truncation error in the spatial discretization with Nth centered approximation $V\frac{\Delta t(\Delta s)^N}{2\times(N+1)!}V^{(N+1)}$ the relative truncation error and the grid spacing limit are

$$Err(N) = (\frac{2\pi\Delta s}{L})^{N+1}\frac{|V|\Delta t}{2\Delta s(N+1)!} \le r_p \quad (6)$$

$$\Delta s \le r_p[\frac{2(N+1)!}{|V|\Delta t}]^{1/N}(\frac{L}{2\pi})^{1+N^{-1}} \quad (7)$$

For the internal tidal wavelength ranges (~20–50 km) in oceans of depths less than 2,000m and r_p =10% (relative error limit), the grid spacing must be less than ~0.1–4km with time step Δt =10~900 seconds and |V| =0.5–2.5m/s for the 2nd and 4th centered approximations (Fig. 2)[20]. Higher spatial resolution (most cases <1km) is needed for longer time steps, shorter wavelengths, or faster flows. It is difficult to see the true tidal effects on climate from the large-scale numerical models due to the much lower resolutions.

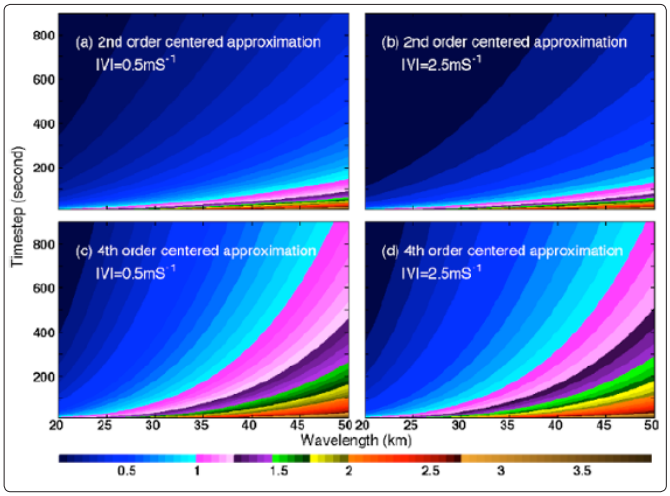

Figure 2: The maximum permitted grid spacing (km) of 2nd (a and b) and 4th (c and d) centered approximations for a 10% relative error limit with different wavelength (km), time step (s), and wave speed (0.5~2.5 ms^{-1}).

Case two on Sun-Moon gravitation induced nonlinear motions of geophysical fluids: Sun-Moon gravitation changes with the relative location between a moving fluid and the Sun or Moon. For a numerical model to determine the location, grid spacing must be smaller than the distance the fluids move within one time step. Pinpointing accurate relative locations between a float and the Sun or Moon, the fast rotation of Earth makes the time step and grid spacing much shorter than those used by classic climate models. If, for example, the time step is one minute and the smallest speed that must be simulated is 0.05m/s (typically for variations of ~10 years), grid spacing must be smaller than 3m [21]. Increasing the time step may enlarge the grid spacing, but results in errors for relative locations and the momentum accumulation effect will be missed.

Well-posed contradiction may exist for internal waves

Well-posedness of numerical solution equires that solution exists, is unique, and changes continuously with the initial condition(s) (stable and convergent if iteration applied) [22]. For stability

$$c\Delta t / \Delta s \leq 1 \tag{8}$$

Equation 8 shows that grid spacing should be proportional to time step for stability required for the well-posed solution, but is inversely proportional to time step in order to limit truncation error during computation of internal waves, as shown in Equation 7. A contradiction exists for the grid spacing between maintaining stability and limiting truncation error.

A new attempt based on relationships of mathematics and physics

Classically, Newton Law was originally written in Lagrangian system, transferred into Eulerian system for continuous space, and then discretized with mixing terms added for sub-grid processes through parameterization with closures dependent of scales, based on speed gradients. Issues mainly come up during the discretization and parameterization.

Here, Newton Law was written in discrete space directly using conservations of momentum and mass, avoiding externally adding mixing terms, and without the parameterization. New discrete momentum and mass equations were established through "mass and momentum-covering relationships (MMCR)" (see Section 3 for details).

Integration of Advection and Mixing Terms

Conservations of momentum and mass derived for discrete fluids

That the micro clusters are both microcosmically big enough and macroscopically small enough is required by the fluid mechanics. The time-step (dt) and size (dx, dy, dz) of fluid micro clusters should be greater than zero for integration. Given a local micro-cluster

$$\mathrm{L} \in \{[x - dx/2,\ x + dx/2]; [y - dy/2, y + dy/2]; [z - dz/2,\ z + dz/2]\} \tag{11}$$

The speed of the local micro-cluster L is $\boldsymbol{V} = u\boldsymbol{i}+v\boldsymbol{j}+w\boldsymbol{k}$ ($\boldsymbol{i}$, $\boldsymbol{j}$, and $\boldsymbol{k}$ are the unit vector in x, y, and z direction respectively). The density of L is ρ at time t=0. Considering $u \geq 0$, $v \geq 0$, and w ≥ 0 at any time $t \in (0, dt]$, the total momentum and mass provided to the local microcluster L by its neighbors (here, all A, B, C, D, E, F, and G were considered; but classically, only A, C and G micro clusters were considered) are respectively (Fig. 3)

$$\boldsymbol{F_m} = \sum_{n=A}^{G} S_n[(\rho_n + \tau\frac{d\rho_n}{dt})(\boldsymbol{V}_n + \tau\frac{d\boldsymbol{V}_n}{dt}) - (\rho + \tau\frac{\partial\rho}{\partial t})(\boldsymbol{V} + \tau\frac{\partial\boldsymbol{V}}{\partial t})] \tag{12}$$

$$M = \sum_{n=A}^{G} S_n[(\rho_n + \tau\frac{d\rho_n}{dt}) - (\rho + \tau\frac{\partial\rho}{\partial t})] \tag{13}$$

where, n can be $A, B, C, D, E, F,$ or G, and

$$\boldsymbol{V}_n = \boldsymbol{V} - (\boldsymbol{R}_n \cdot \nabla)\boldsymbol{V} \tag{14}$$

$$\rho_n = \rho - \boldsymbol{R}_n \cdot \nabla\rho \tag{15}$$

$$\boldsymbol{R}_A = \boldsymbol{i}dx \tag{16}$$

$$\boldsymbol{R}_B = \boldsymbol{i}dx + \boldsymbol{j}dy \tag{17}$$

$$\boldsymbol{R}_C = \boldsymbol{j}dy \tag{18}$$

$$\boldsymbol{R}_D = \boldsymbol{i}dx + \boldsymbol{k}dz \tag{19}$$

$$\boldsymbol{R}_E = \boldsymbol{i}dx + \boldsymbol{j}dy + \boldsymbol{k}dz \tag{20}$$

$$\boldsymbol{R}_F = \boldsymbol{i}dy + \boldsymbol{k}dz \tag{21}$$

$$\boldsymbol{R}_G = \boldsymbol{k}dz \tag{22}$$

Covering volumes at time t of micro-clusters A to G are

$$S_A = \tau(u_A + \tau du_A/dt)\,[dy - \tau(v_A + \tau dv_A/dt)]\,[dz - \tau(w_A + \tau dw_A/dt)] \tag{23}$$

$$S_C = \tau\,[dx - \tau(u_C + \tau du_C/dt)](v_C + \tau dv_C/dt)\,[dz - \tau(w_C + \tau dw_C/dt)] \tag{24}$$

$$S_C = \tau\,[dx - \tau(u_C + \tau du_C/dt)](v_C + \tau dv_C/dt)\,[dz - \tau(w_C + \tau dw_C/dt)] \tag{25}$$

$$S_D = \tau^2(u_D + \tau du_D/dt)\,[dy - \tau(v_D + \tau dv_D/dt)]\,(w_D + \tau dw_D/dt) \tag{26}$$

$$S_E = \tau^3(u_E + \tau du_E/dt)\,(v_E + \tau dv_E/dt)(w_E + \tau dw_E/dt) \tag{27}$$

$$S_F = \tau^2[dx - \tau(u_F + \tau du_F/dt)](v_F + \tau dv_F/dt)\,(w_F + \tau dw_F/dt) \tag{28}$$

$$S_G = \tau[dx - \tau(u_G + \tau du_G/dt)]\,[dy - \tau(v_G + \tau dv_G/dt)]\,(w_G + \tau dw_G/dt) \tag{29}$$

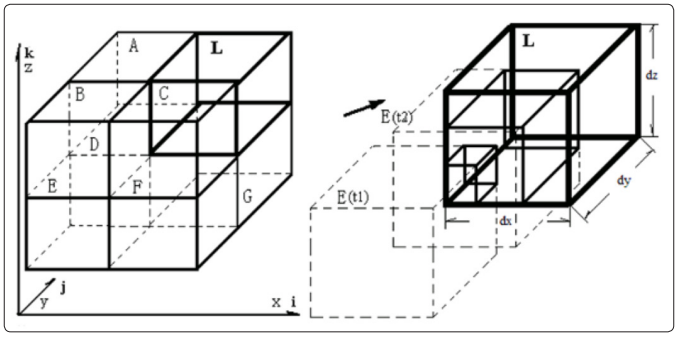

Figure 3: Diagrams for the coverage relationship among the fluid micro-clusters with the local one marked as L of size of dx, dy, and dz and its neighboring ones marked as A, B, C, D, E, F, G, and H, respectively.

Kinetic equations for discrete fluids

Defining the momentum-transporting compensative speed as

$$\boldsymbol{V}_\rho \equiv \boldsymbol{i}u_\rho + \boldsymbol{j}v_\rho + \boldsymbol{k}w_\rho \tag{30}$$

$$u_\rho = \frac{dx}{\rho}\left(dx\frac{\partial\rho}{\partial x}\frac{\partial u}{\partial x} - \frac{\partial\rho u}{\partial x}\right) \tag{31}$$

$$v_\rho = \frac{dy}{\rho}\left(dy\frac{\partial\rho}{\partial y}\frac{\partial v}{\partial y} - \frac{\partial\rho v}{\partial y}\right) \tag{32}$$

$$w_\rho = \frac{dz}{\rho}\left(dz\frac{\partial\rho}{\partial z}\frac{\partial w}{\partial z} - \frac{\partial\rho w}{\partial z}\right) \tag{33}$$

Eq. 30 represents the compensated momentum transport of the speed resulting from the spatially uneven distribution of density and speed.

Defining the momentum-transporting speed as

$$\boldsymbol{V}_r \equiv \boldsymbol{i}dx\,\partial u/\partial x + \boldsymbol{j}dy\,\partial v/\partial y + \boldsymbol{k}dz\partial w/\partial z \tag{34}$$

Using Eq. 12, the total impulsive force per unit of volume of the local micro-cluster is

$$\boldsymbol{F} = \lim_{\tau \to 0} \boldsymbol{F}_m/(\tau\times dx\times dy\times dz)$$

$$= \boldsymbol{V}[(\boldsymbol{V}_r - \boldsymbol{V})\cdot\nabla\rho] - \rho\left[(\boldsymbol{V}_\rho + \boldsymbol{V})\cdot\nabla\right]\boldsymbol{V} \tag{35}$$

By applying Newton mechanics to an instantaneous covering fluid, I rewrote the fluid mechanics kinetic equations as following:

$$\partial\boldsymbol{V}/\partial t + \left[(\boldsymbol{V}+\boldsymbol{V}_\rho)\cdot\nabla\right]\boldsymbol{V} = -\rho^{-1}\nabla p + \boldsymbol{G_o} \tag{36}$$

Advection terms become

$$(\boldsymbol{V}\cdot\nabla)\boldsymbol{V} \equiv \boldsymbol{i}\left(u\frac{\partial}{\partial x} + v\frac{\partial}{\partial y} + w\frac{\partial}{\partial z}\right)u + \boldsymbol{j}\left(u\frac{\partial}{\partial x} + v\frac{\partial}{\partial y} + w\frac{\partial}{\partial z}\right)v + \boldsymbol{k}(u\frac{\partial}{\partial x} + v\frac{\partial}{\partial y} + w\frac{\partial}{\partial z})w \tag{37}$$

$$(\boldsymbol{V}_\rho\cdot\nabla)\boldsymbol{V} \equiv \boldsymbol{i}\left(u_\rho\frac{\partial}{\partial x} + v_\rho\frac{\partial}{\partial y} + w_\rho\frac{\partial}{\partial z}\right)u + \boldsymbol{j}\left(u_\rho\frac{\partial}{\partial x} + v_\rho\frac{\partial}{\partial y} + w_\rho\frac{\partial}{\partial z}\right)v + \boldsymbol{k}(u_\rho\frac{\partial}{\partial x} + v_\rho\frac{\partial}{\partial y} + w_\rho\frac{\partial}{\partial z})w \tag{38}$$

where, $\boldsymbol{G}_o$ is the composite force of all the other forces except pressure gradient force, p is the classical pressure used in kinetic and state equations, also known as hydrostatic pressure.

$(\boldsymbol{V}\cdot\nabla)\,\boldsymbol{V}$ in Eq. 37 is the classical advection term, while $(\boldsymbol{V}\mathrm{p}\cdot\nabla)\,\boldsymbol{V}$ in Eq. 38 is a higher-order spatial advection term and is induced from the spatial unevenness in both density and speed (e.g., drops carried by spatially uneven wind in density or speed will provide impulsive force to the neighboring air), and can be large for the fluids with slow speed and large momentum or density unevenness, e.g., in costal and tropical regions.

The force or transport from the higher-order spatial advection term is kind of "mixing", proportional to speed gradients with coefficients of u_p, v_p, and w_p that are functions of density, grid spacing (clusters' size will be set as grid spacing in x, y, and z directions, respectively), and the gradients of speed, density and momentum. No parameterization is required and grid effects will be automatically computed according to grid spacing and gradients during numerical modeling. Much higher resolutions will be required, which is being supported by today's developed computation capacity.

Eq. 36 can be written into the classical form of momentum equation as

$$\partial\boldsymbol{V}/\partial t + (\boldsymbol{V}\cdot\nabla)\boldsymbol{V} = -\boldsymbol{\rho}^{-1}\nabla p_c + \boldsymbol{G_o} \tag{39}$$

where,

$$p_c = p + \nabla^{-1}[\rho(\boldsymbol{V}_\rho\cdot\nabla)\boldsymbol{V}] \tag{40}$$

Here, the higher-order spatial advection term become the "kinetic pressure" as defined in the on the right-hand side of Eq. 40, result from the uneven spatial distribution of fluid density and speed on basis of the relative motion, not from thermal motion of molecules or weight of fluids. Hence, p_c is no longer just the classical hydrostatic pressure p unless fluid is even or at rest.

If continuous fluids are mathematically abstracted as $dx=0$, $dy=0$, and $dz=0$, the higher-order spatial derivative disappears. However, "micro-clusters" of zero volume cannot contribute to real fluid space. Therefore fluid mechanics requires that the micro-cluster should be both microcosmically big enough and macroscopically small enough.

Continuity equation for discrete fluids without mass source or sink

Using Eq. 13, omitting mass source or sink, omitting compressibility of fluids, the total rate of mass increase of the local micro-cluster is contributed from its neighbors for per unit of volume and is

$$\partial\rho/\partial t = \lim_{\tau \to 0} M/(\tau \times dx \times dy \times dz)$$
$$= (\boldsymbol{V}_r - \boldsymbol{V}) \cdot \nabla\rho \quad (41)$$

Or I wrote the continuation equation for fluids as

$$\frac{\partial\rho}{\partial t} + (\boldsymbol{V} - \boldsymbol{V}_r) \cdot \nabla\rho = 0 \quad (42)$$

The impulsive force and mass provided to the local fluid micro-cluster by its neighbors are result from both the relative motion and spatially uneven distribution of fluid density and speed. The momentum and mass covering relationships among fluid micro-clusters of size ($dx \times dy \times dz$) are same as those among fluid clusters of size $\Delta x \times \Delta y \times \Delta z$.

Modification of kinetic equations for discrete fluids

In classical discrete fluid kinetic equations, Δx, Δy, Δz, and Δt represent the grid spacing and time step in x, y, z and directions, respectively. Such definitions, however, do not meet mathematical requirements, that are: $\Delta x = u\Delta t$, $\Delta y = v\Delta t$, $\Delta z = w\Delta t$, and correspondingly $\Delta_d E/\Delta d = \partial E/\partial d$ (the difference of element E, with E=u, v, w, or p, in d-direction, with d = x, y, z, or t. $\Delta_d E$ is the increment of E in d-direction within Δd). The changing speed and constant grid spacing make it impossible for the practical discretization to meet the mathematical requirements (see †3 for details).

The certainty for the MMCR physically requires time-steps that must be short enough to guarantee that the distance for fluids to move within one time-step is shorter than the grid spacing, i.e.

$$MAX\{|u\Delta t/\Delta x|, |v\Delta t/\Delta y|, |w\Delta t/\Delta z|\} \le 1 \quad (43)$$

For the discrete fluid kinetic equations

$$\Delta\boldsymbol{V}/\Delta t + \left[(\boldsymbol{V}+\boldsymbol{V}_\rho) \cdot \nabla\right]\boldsymbol{V} = -\rho^{-1}\nabla p + \boldsymbol{G_o} \quad (44)$$

$$u_\rho = \rho^{-1}[\Delta_x\rho\Delta_x u - \Delta_x(\rho u)] \quad (45)$$

$$v_\rho = \rho^{-1}[\Delta_y\rho\Delta_y v - \Delta_y(\rho v)] \quad (46)$$

$$w_\rho = \rho^{-1}[\Delta_z\rho\Delta_z w - \Delta_z(\rho w)] \quad (47)$$

$$\left[(\boldsymbol{V}+\boldsymbol{V}_\rho) \cdot \nabla\right]\boldsymbol{V} = \boldsymbol{i}\left[(u+u_\rho)\Delta_x u/\Delta x + (v+v_\rho)\Delta_y u/\Delta y + (w+w_\rho)\Delta_z u/\Delta z\right]$$

$$+\boldsymbol{j}\left[(u+u_\rho)\Delta_x v/\Delta x + (v+v_\rho)\Delta_y v/\Delta y + (w+w_\rho)\Delta_z v/\Delta z\right]$$

$$+\boldsymbol{k}\left[(u+u_\rho)\Delta_x w/\Delta x + (v+v_\rho)\Delta_y w/\Delta y + (w+w_\rho)\Delta_z w/\Delta z\right]$$

Marking each difference term of the main spatial derivative $-(\boldsymbol{V} \cdot \nabla)\boldsymbol{V}$ at the local grid point as

$$F_{ij} = -q_j(\Delta_j q_i)/L_j \quad (49)$$

where, $L_j = \Delta x$, Δy, or Δz, q_i or $q_j = u$, v, or w.

For simplicity, let m be the grid coordinate in i-direction and n in j-direction. F_{ij} is the i-direction force component contributed by the j-direction advection of q_i to the local fluid block Fig. 4), which equals the one unit mass momentum-transporting rate of this block according to the momentum law. However, even if the speed at a grid point can represent the averaged speed within that grid box, the discrete fluid must cover a distance equal to the grid spacing within one time step in order to calculate the corresponding momentum, which works against the discretization precondition (Eq. 43). In this sense, momentum law was not calculated correctly in the classical discrete scheme.

To calculate the momentum law correctly and keep the discretization precondition (Eq. 4), the speed used to calculate momentum must be the speeds at the bordering walls (m±1/2, n±1/ 2) of the local block and the F_{ij} should be calculated by application of the momentum-covering relationship.

If $i=j$ $(m=n)$,

$$F_{ij} = \frac{1}{L_i}\{{q_i}^2[m-\tfrac{1}{2},n] - {q_i}^2[m+\tfrac{1}{2},n]\} \quad (50)$$

If $i \neq j$ $(m \neq n)$,

$$F_{ij} = \frac{1}{L_i}\{q_i[n-\tfrac{1}{2},m]q_j[n-\tfrac{1}{2},m] - q_i[n+\tfrac{1}{2},m]q_j[n+\tfrac{1}{2},m]\} \quad (51)$$

To calculate the mean speeds at the bordering walls of the local block without knowing its local change with time, two potential calculation schemes were suggested below.

One, simple arithmetical scheme: If within the distance the fluid covers within one time step, the speed change is very small (for instance, to calculate the slow-speed fluids with small spatial gradient), the mean speed at the bordering walls of the local block in i- and j-directions are given by

$$q_i[m \pm \tfrac{1}{2},n] = \tfrac{1}{2}\{q_i[m \pm \tfrac{1}{2},n] + q_i[m,n]\} \quad (52)$$

$$q_i[n \pm \tfrac{1}{2},m] = \tfrac{1}{2}\{q_i[n \pm 1,m] + q_i[n,m]\} \quad (53)$$

$$q_j[n \pm \tfrac{1}{2},m] = \tfrac{1}{2}\{q_j[n \pm 1,m] + q_j[n,m]\} \quad (54)$$

Two, time-step-dependent scheme: If within the distance the fluid covers within one time step, the speed change is not very small (for instance, to calculate the high-speed fluids and/or with big spatial gradient), the mean speed at the bordering walls of the local block in i- and jdirections can be calculated according to the real distance the fluid covers

$$q_i[m \pm \tfrac{1}{2},n] = \frac{q_i[m\pm1,n]+q_i[m,n]}{2}\left\{1 \pm \Delta t\frac{q_i[m,n]-q_i[m\pm1,n]}{2L_i}\right\}$$

$$+\Delta t\frac{q_j[m\pm1,n]+q_j[m,n]}{8L_j}$$

$$\times\{q_i[m\pm1,n-1]+q_i[m,n-1]-q_i[m\pm1,n+1]$$

$$-q_i[m,n+1]\} \quad (55)$$

$$q_i[n\pm\frac{1}{2},m]=\frac{q_i[n\pm1,m]+q_i[n,m]}{2}$$

$$\left\{1+\Delta t\frac{q_i[n\pm1,m-1]+q_i[n,m-1]-q_i[n\pm1,m+1]-q_i[n,m+1]}{4L_i}\right\}$$

$$\pm\Delta t\frac{q_j[n\pm1,m]+q_j[n,m]}{4L_j}\{q_i[n,m]-q_i[n\pm1,m]\} \quad (56)$$

$$q_j[n\pm\frac{1}{2},m]=\frac{q_j[n\pm1,m]+q_j[n,m]}{2}\left\{1\pm\Delta t\frac{q_j[n,m]-q_j[n\pm1,m]}{2L_j}\right\}$$

$$+\Delta t\frac{q_i[n\pm1,m]+q_i[n,m]}{4L_i}$$

$$\times\{q_j[n\pm1,m-1]+q_j[n,m-1]-q_j[n\pm1,m+1]$$

$$-q_j[n,m+1]\} \quad (57)$$

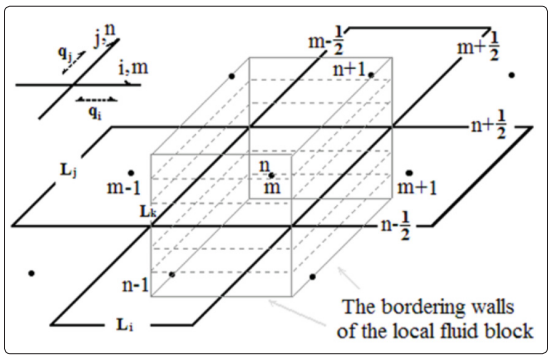

Figure 4: Diagram for the discrete grid scheme

Examination through Numerical experiments

Here the preliminary effect for using the MMCR was examined through the Lamont Ocean-AML (atmospheric mixed layer) Model (LOAM) with the time-step-dependent scheme. LOAM is developed from the original Gent-Cane model, using primitive equations [17]. At its core, LOAM uses: the hydrostatic balance, the rigid-lid approximation, the fourth-order centered differencing in the horizontal, fourth order temporal Lorenz cycle, and convective adjustment with wind stirring assuming a Richardson-number dependent mixing [23]. Model calculations are performed on stretched longitude/latitude A-grid with a 50~200km horizontal resolution covering a 20°S- 20°N latitude zone with 28 ocean depth (m) levels (5, 15, 25, 35, 45, 55, 65, 75, 85, 95, 110, 130, 170, 220, 300, 390, 490, 600, 800,1000,1500, 2000, 2500, 3000, 3500, 4000, 4500, 5000) and a time step of 30 minutes. Experiments employed data of CMAP (CPC Merged Analysis of Precipitation) monthly precipitation, sea surface temperature from NCAR (National Center for Atmospheric Research), Levitus salinity, air temperature, moisture, wind, wind stress, geopotential height, and sea surface heat fluxes from the NCEP reanalysis (provided by NOAA CIRES Climate Diagnostics Center). The longwave, sensible, and latent heat fluxes were computed from LOAM, using formulation of Seager and Blumenthal and the mixed layer formulation of Chen et al. [24-25].

For a preliminary examination of the MMCR, two experiments were conducted with ("new scheme") and without ("old scheme") the MMCR for calculating the advection and convection terms in the momentum equations and all the other parameters were kept intact. LOAM was optimized according to the old scheme and was run at large spatial scales, which minimizes the contribution of advection and convection, and will therefore restrict the effect of the new scheme. Even though the new scheme showed better skills in simulations of sea surface temperatures, especially within tropical oceans where the uneven ness of fluid momentum is larger (Fig. 5), based on modeling results for a period of 1979–2002.

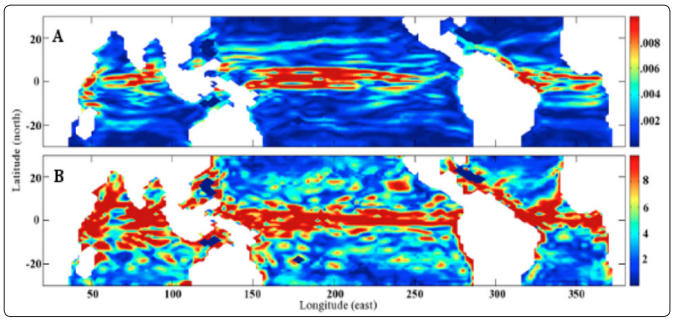

Figure 5: Spatial unevenness expressed with surface horizontal momentum gradient (kgm^{-3}s $^{-1}$, **A**) and compensative speed (ms^{-1}, **B**) in the tropical oceans, computed from the monthly output in May 2000 from Lamont Ocean-Atmosphere Model (50-200km resolution).

The correlation between the average observed and simulated sea surface temperatures increased by 6%, 18%, 14%, 22%, and 4% averaged in the equatorial (5°S-5°N) Niño3 (210°-270°E), warm pool (120°-160°E), Atlantic (320°-360°E), Indian (40° -100°E), and the entire region, respectively (Fig. 6). The 1979-2002 mean simulated sea surface temperatures were more closely matched to observations across our entire domain if using the new scheme than if using the old scheme (Fig. 7). The MMCR did improve modeling for the momentum-uneven fluids as it was supposed to be.

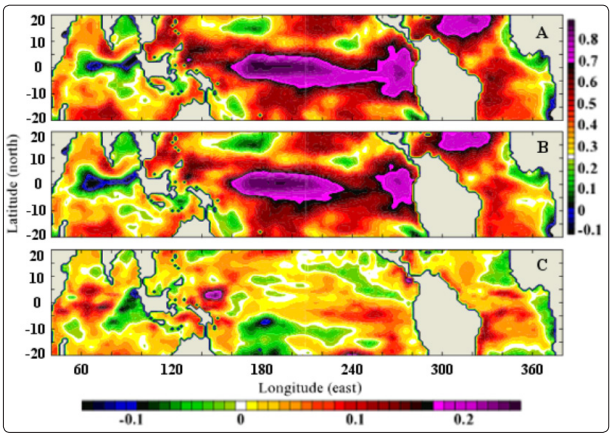

Figure 6: Correlations between NCAR-observed and LOAM-simulated sea-surface temperatures for new scheme (**A**), old scheme

(**B**), and the difference with new minus old scheme (**C**).

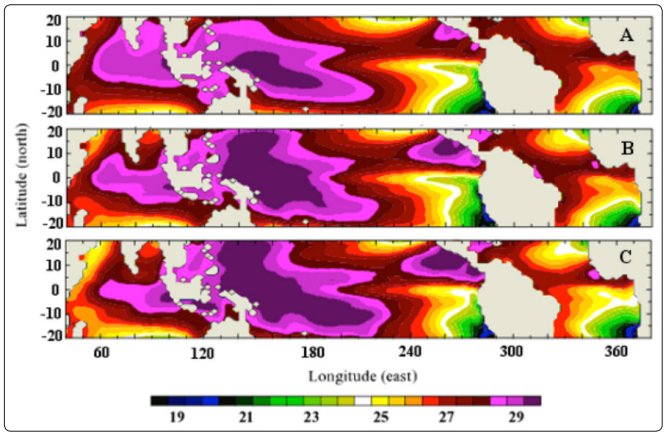

Figure 7: Comparison of mean NCAR-observed sea-surface temperatures (**A**) and simulated sea-surface temperatures using old/new discretization scheme ( ) for period of 1979-2002.

Summary and Discussion

During the application of Newton Law for discrete fluids in Eulerian system, momentum-unevenness of fluids may cause modeling uncertainties due to mathematical discretization, improper resolutions, parameterized mixing, and other modeling processes such as smoothing and filtering. First, two mathematical preconditions for the discretization have not been met in modeling due to mathematical misrepresentations where the grid spacing has been automatically (wrongly) set as the distance for fluids to move within one time-step. Second, the lower resolutions have linearized, rather extensively, nonlinear motions and may have failed to forecast accelerations that can cause climate adjustments. Resolutions of large-scale numerical models are far from sufficiency to have accurate solutions for tide-associated dynamics, because numerically solving internal waves or pinpointing accurate relative locations between fluids and the Sun or Moon for solving the nonlinear Sun-Moon driven fluid system requires much higher resolutions due to the fast wave speed or the fast rotation of Earth (e.g., grid spacing can be smaller than 3m). Well-posed contradiction for discrete fluids may be caused with improper (lower) resolutions. Third, local parameterizations for subscale behaviors with various closures may cause uncertainties in mixing.

In order to avoid mixing parameterizations that are locally dependent of modeling domains, grids, and processes, here I wrote Newton Law directly for discrete fluids under conservations of momentum and mass using "mass and momentum-covering relationships (MMCR)". Accordingly, new discrete momentum and mass equations were established with new views and schemes. First, advection and mixing can be integrated together and mixing is the higher-order spatial advection term induced from speed gradients times coefficients that are functions of density, grid spacing, and the gradients of speed, density and momentum. Second, parameterization can be avoided, and no uncertain parameters need be involved in modeling. Third, the certain MMCR among fluid micro-clusters imply a precondition that the neighboring fluid micro-clusters should not pass over the local fluid micro-cluster within one time-step, as is required for classical discretization.

When applied over tropical oceans where momentum unevenness is larger, the discretization scheme derived from MMCR improved the modeling of sea surface temperatures by simply using this scheme to calculate the advection and convection terms in the momentum equations. However, more experiments need to be performed for multiple models using multiple resolutions without and with multiple mixings in order to fully evaluate and compare modeling effects and computing efficiencies. Unfortunately, there are no facility and funding available for me to perform this study further.

References

1. Wang Z (2016) Preliminary studies of climate-environment dynamics for our Climate Prediction and Environment, Outskirt Press ISBN 9781478779032, p 308.
2. Wang Z, D Wu, X Chen, R Qiao (2012B) ENSO Indices and Analysis, Adv. in Atmo. Sci 30: 1491-1506.
3. Mellor G L, T Yamada (1974) A hierarchy of turbulent closure models for planetary boundary layers, J. Atmos. Sci 31: 1791-1806.
4. Mellor G L, T Yamada (1982) Development of a turbulence closure model for geophysical fluid problems, Rev. Geophys 20: 851-875.
5. Blumberg A F, B G Galperin, D J O'Connor (1992) Modeling vertical structure of open channel flow, J. Hydraul. Eng 118: 1119-1134.
6. Large W G, P R Gent (1999) Validation of vertical mixing in an equatorial ocean model using large eddy simulations with observations, J. Phys. Oceanogr 29: 449-464.
7. Price J F, R F Weller, R Pinkel (1986) Diurnal cycling: Observations and models of the upper ocean response to diurnal heating, cooling and wind mixing, J. Geophys. Res 91: 8411-8427.
8. Chen D, L M Rothstein, A J Busalacchi (1994) A hybrid vertical mixing scheme and its application to tropical ocean models. J. Phys. Oceanogr 24: 2156-2179.
9. Large W G, J C McWilliams, S C Doney (1994) Oceanic vertical mixing: A review and a model with a nonlocal boundary layer parameterization, Rev. Geophys 32: 363-403.
10. Kantha L H, C A Clayson (1994) An improved mixed layer model for geopysical applications, J. Geophys. Res., 99, 25: 235–266.
11. Burchard H, K Bolding (2001) Comparative analysis of four second moment turbulence closure models for the oceanic mixed layer, J. Phys. Oceanogr 31: 1943-1968.
12. Wijesekera H, J Allen, P Newberger (2003) Modeling study of turbulent mixing over the continental shelf: Comparison of turbulent closure schemes, J. Geophys. Res doi:10.1029/2001JC001234.
13. Durski S M, S M Glenn, D B Haidvogel (2004) Vertical mixing schemes in the coastal ocean: Comparison of the level 2.5 Mellor-Yamada scheme with an enhanced version of the K profile parameterization, J. Geophys. Res doi: 10.1029/2002JC001702.
14. Philip A Thompson (1988) Compressible-Fluid Dynamics, Rensselaer Polytechnic Institute Press.
15. Pijush K Kundu, Ira M Cohen (2002) Fluid Mechanics, 2nd Ed Academic Press.
16. Shapiro R (1970) Smoothing, filtering, and boundary effects, Rev. Geophys. And Space Physics, 8: 359-387.
17. Gent P R, M A Cane (1989) A reduced gravity, primitive equation model of the upper equatorial ocean. J. Comput Phys. 81: 444-480.
18. Barnston A G (1994) Long-lead Seasonal Forecasts: Where do

we stand? Bull. Am. Meteorol. Soc 75: 2097-2114.
19. Iskandarani M, D B Haidvogel, J Levin, E Curchitser, C A Edwards (2002) Multiscale geophysical modeling using the spectral element method. Comp. Sci. Eng 4: 42-48.
20. Robertson R, A Field (2005) M2 baroclinic tides in the Indonesian Seas. Oceanography, 18: 62-73.
21. Wang Z, D Wu, X Song, X Chen, S Nicholls (2012A) Sun-Moon Gravitation Induced Wave Characteristics and Climate Variation. J. Geophys. Res doi.org/10.1029/2011JD016967.
22. Jacques H (1902) Sur les problèmes aux dérivées partielles et leur signification physique. Princeton University Bulletin 13: 49-52.
23. Lorenz E N, An N-cycle time differencing scheme for stepwise numerical integration, Mon.Wea.Rev 99: 644-648.
24. Seager, Blumenthal (1994) Modeling tropical Pacific sea surface temperature with satellite-derived solar radiative forcing. Journal of Climate 7: 1943-1957.
25. Chen D, L M Rothstein, A J Busalacchi, L M Rothstein (1994) The roles of vertical mixing, solar radiation, and wind stress in a model simulation of the sea surface temperature seasonal cycle in the tropical Pacific ocean, J. Geophys. Res 99: 20345-20359.